Journal of Solid State Chemistry 184 (2011) 1393–1399

Contents lists available at ScienceDirect

Journal of Solid State Chemistry

journal homepage: www.elsevier.com/locate/jssc

An *in situ* oxidation route to fabricate graphene nanoplate–metal oxide composites

Sheng Chen, Junwu Zhu *, Xin Wang *

Key Laboratory of Soft Chemistry and Functional Materials, Nanjing University of Science and Technology, Ministry of Education, Nanjing 210094, PR China

ARTICLE INFO

Article history:
Received 10 December 2010
Received in revised form
21 March 2011
Accepted 29 March 2011
Available online 13 April 2011

Keywords:
Graphene
Metal oxide
Metal nitrate
Soft oxidation
Hydrolysis

ABSTRACT

We report our studies on an improved soft chemical route to directly fabricate graphene nanoplate–metal oxide (Ag_2O, Co_3O_4, Cu_2O and ZnO) composites from the *in situ* oxidation of graphene nanoplates. By virtue of H^+ from hydrolysis of the metal nitrate aqueous solution and NO_3^-, only a small amount of functional groups were introduced, acting as anchor sites and consequently forming the graphene nanoplate–metal oxide composites. The main advantages of this approach are that it does not require cumbersome oxidation of graphite in advance and no need to reduce the composites due to the lower oxidation degree. The microstructures of as-obtained metal oxides on graphene nanoplates can be dramatically controlled by changing the reaction parameters, opening up the possibility for processing the optical and electrochemical properties of the graphene-based nanocomposites.

1. Introduction

Since the discovery of graphene in 2004, this wonder material has attracted ever increasing attention owning to its novel electrical performances and unique properties [1,2]. To explore the potential applications of graphene, different synthetic techniques, such as liquid-phase exfoliation of graphite [3], chemical vapor deposition [4–6], self-assembly approach [7] and chemical reduction of graphite oxide [8] have been extensively developed to produce mono- and few-layer graphene sheets in bulk quantities. It is demonstrated that the incorporation of graphene sheets into composite materials is an effective way to harness these intriguing properties [9].

Currently, the main interests in preparing graphene based hybrids are concentrated on exfoliating graphene through a heavy oxidation, followed by reduction through chemical methods (Fig. 1a) [9–12]. Nevertheless, in this laborious procedure, some environmental incompatible agents are widely used; producing a large amount of framework defects during the deoxygenation of GO is inevitable [9–12]. The conductivity of the reduced GO is severely impaired by the defects and the purity of the composite is decreased due to the fragments [13–15].

The fact is that GO is heavily oxygenated graphene bearing plenty of oxygen-containing groups, but only a part of these functional groups play a role in anchoring metal ions to form graphene oxide based nanostructures [13]. The reduction process is used mainly to eliminate the redundant functional groups on graphene sheets [16]. A seemingly obvious prediction is that a more straightforward route can be developed *via* direct oxidation of pristine graphene under gentle conditions, so that relatively small amounts of functional groups are produced as the anchor sites to decorate graphene plates with nanoparticles (Fig. 1a). One feature of such process is that there is no need to reduce the composites because of the low oxidation degree, ultimately leading to a carbon framework with a lower defect density.

In recent years, inorganic materials, such as Fe_3O_4, Co_3O_4, Cu_2O, ZnO and Ag_2O, have attracted ever-increasing attention for their widely utilization in catalysts, water purification, hydrogen production, lithium ion batteries, transparent electronics, *etc.* [17–21]. Taking into account the excellent properties of graphene, such as a large theoretical specific surface area (2630 $m^2\ g^{-1}$) [22], high values of Young's modulus (~1.1 Tpa), excellent thermal conductivity (~5000 $W\ m^{-1}\ s^{-1}$) and amazing intrinsic mobility (200,000 $cm^2\ v^{-1}\ s^{-1}$) [16] the combination of graphene with these nanoparticles may give enhanced performances.

Herein, we report our studies on an improved soft chemical route to directly fabricate graphene nanoplate–metal oxide (Ag_2O, Co_3O_4, Cu_2O and ZnO) composites from the *in situ* oxidation of graphene nanoplates. The novelty of this work is using H^+ from the hydrolysis of metal nitrate in conjunction with NO_3^- to introduce oxygen-containing groups on graphene sheets; thereby an *in situ* approach to absorbing metal oxide nanoparticles onto graphene nanoplates is created (Fig. 1b). The H^+ concentration is much lower

* Corresponding authors. Fax: +86 25 8431 5054.
E-mail addresses: zhujw@mail.njust.edu.cn (J. Zhu), wxin@public1.ptt.js.cn (X. Wang).

0022-4596/$ - see front matter © 2011 Elsevier Inc. All rights reserved.
doi:10.1016/j.jssc.2011.03.054

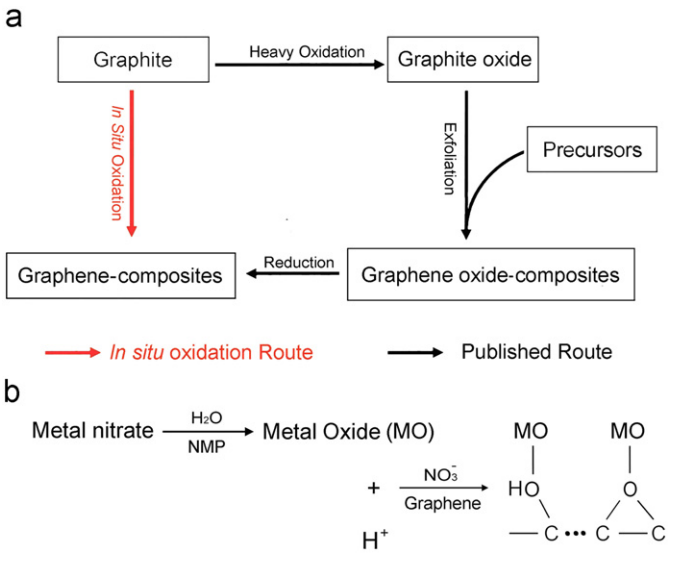

Fig. 1. (a) Comparison of as-proposed *in situ* oxidation route with the published route for the synthesis of graphene based composites and (b) the proposed reactions for the formation of graphene–metal oxide composites.

compared with that of traditional oxygenation processes (where strong oxidation reagents, such as sulfuric acid, nitric acid, *etc.*, were used), therefore this oxidation route is considered to be much softer.

2. Material and methods

2.1. Preparation

2.1.1. Synthesis of graphene dispersion

Graphene sheets were produced by dispersion and exfoliation of bulk graphite in N-Methyl-2-pyrrolidone (NMP) at a starting concentration of 0.1 mg mL^{-1} according to Hernandez et al. [23]. Specifically, natural graphite (20 mg) was dispersed in NMP (200 mL) with sonication in a low power sonic bath for 30 min. The resultant dispersion was then centrifuged for 90 min at 500 rpm. Afterwards, decantation was carried out by pipetting off the top half of the dispersion. A homogeneous dark dispersion was obtained and used as the starting material. The main components of graphene dispersion are NMP and exfoliated graphene sheets [23]. A graphene sheet has a characteristic thickness of 1–5 nm and a lateral size of several micrometers [16].

2.1.2. Synthesis of graphene–Ag_2O nanocomposites

The as-obtained graphene dispersion (100 mL) was vigorously stirred, while $AgNO_3$ aqueous solution (7.5 mL) was introduced rapidly. The mixture was kept standing in a covered beaker under ambient conditions for some time. The product was finally centrifuged, washed and dried at 60 °C. For reliable comparison, three $AgNO_3$ solutions with different reaction duration were prepared, namely 2 mg mL^{-1} for 10 min (GA-1), 20 mg mL^{-1} for 4 h (GA-2) and 200 mg mL^{-1} for 72 h (GA-3), respectively.

2.1.3. Synthesis of graphene–Co_3O_4 nanocomposites

A $Co(NO_3)_2 \cdot 6H_2O$ aqueous solution (200 mg of $Co(NO_3)_2 \cdot 6H_2O$ dissolved in 5 mL of de-ioned water) was added into 100 mL of graphene dispersion with vigorously stirring. The mixture was loaded into a Teflon-lined stainless steel autoclave and heated at 180 °C for 2 h. After being cooled to room temperature, the black precipitate was collected and washed with DI-water and ethanol three times, and dried at 60 °C.

2.1.4. Synthesis of graphene–ZnO nanocomposites

The as-prepared graphene dispersion (100 mL) was stirred in a round-bottomed flask equipped with a refluxing apparatus, where $Zn(NO_3)_2$ aqueous solution (200 mg of $Zn(NO_3)_2$ dissolved in 5 mL of de-ioned water) was added. The solution was heated to 120 °C with vigorous stirring for 2 h. The graphenes with ZnO on them were then separated by centrifuge, washed and dried at 60 °C.

2.1.5. Synthesis of graphene–Cu_2O nanocomposites

The synthesis of graphene–Cu_2O nanocomposites is similar to that of graphene–ZnO. Specifically, $Cu(NO_3)_2$ aqueous solution (200 mg of $Cu(NO_3)_2 \cdot 3H_2O$ dissolved in 5 mL of de-ioned water) was dispersed in the as-prepared graphene dispersion (100 mL) and heated to 120 °C with vigorous stirring for 2 h. The as-obtained product was centrifuged, washed and dried at 60 °C.

2.2. Microstructural characterization

Powder X-ray diffraction (XRD) analyses were performed on a Bruker D8 Advance diffractometer with Cu $K\alpha$ radiation ($\lambda \approx 1.54$ Å). Raman spectra were run on a Renishaw Raman microscope. FT-IR spectra of KBr powder pressed pellets were recorded on a Bruker VECTOR 22 spectrometer. Morphologies of as-obtained products were observed on a transmission electron microscope (TEM, JEOL JEM-2100) and field emission scanning electron microscopy (FESEM, LEO-1550). X-ray photoelectron spectra (XPS) were recorded on a Perkin-Elmer PHI5000C X-ray photoelectron spectrometer, using Mg $K\alpha$ ($h\upsilon = 1253.6$ eV) X-ray as the excitation source.

2.3. Electrochemical characterization

The electrochemical properties of as-obtained products were characterized by cyclic voltammetry (CV), electrochemical impedance spectroscopy (EIS) and galvanostatic charge–discharge measurements. The CV and EIS were analyzed in a three-electrode configuration on a CHI 660C electrochemical workstation (Shanghai CH Instrument Company, China); galvanostatic charge–discharge measurements were analyzed in a two-electrode configuration in a VMP2/Z multi-channel potentiostat/galvanostat (Princeton Applied Research).

In a three-electrode cell, the working electrodes were fabricated by mixing the prepared powders with 15 wt% acetylene black and 5 wt% polytetrafluorene–ethylene (PTFE) binder. A small amount of DI-water was added to the mixture to produce a homogeneous paste. The mixture was pressed onto nickel foam current-collectors (1.0 cm × 1.0 cm) to make electrodes. The mass of GA-1, GA-2 and GA-3 is 2.8, 4.2 and 4.3 mg, respectively. Before the electrochemical test, the prepared electrode was soaked overnight in a 6 M KOH solution. Platinum foil and a saturated calomel electrode (SCE) were used as the counter and reference electrodes, respectively.

In a two-electrode cell, prototype supercapacitors were assembled in a symmetrical two-electrode configuration [24]. The as-obtained samples were mixed with 15 wt% acetylene black and 5 wt% PTFE binder. The mixture was attached on two Pt foils with the same weight. At the end of the Pt foil, a platinum wire was clipped onto the foil by a toothless alligator clip, which was then connected to a VMP2/Z multi-channel potentiostat/galvanostat (Princeton Applied Research) for electrochemical characterization. The mass of GA-3 in one electrode is 2.0 mg.

3. Results and discussion

Silver oxide has a long history of performing well in glucose sensors, oxidants, precursors for fabricating Ag nanoparticles, mediated catalysts and electrochemically active materials [20,25]. As will be discussed later, Ag_2O nanoparticles can be produced from $AgNO_3$ hydrolyzed in a water–NMP system [20]. The H^+ and NO_3^- ions yielded from the hydrolysis can react with carbon atoms of graphene sheets to form oxygen-containing functional groups, which can coordinate with metal ions, playing the role of anchor (Fig. 1b). For reliable comparison, three $AgNO_3$ solutions with different reaction duration were prepared, namely 2 mg mL^{-1} for 10 min (GA-1), 20 mg mL^{-1} for 4 h (GA-2) and 200 mg mL^{-1} for 72 h (GA-3) (please see Section 2).

The starting material graphene sheets were obtained from dispersion and exfoliation of bulk graphite in N-methyl-pyrrolidone (NMP) according to the method of Hernandez et al. [23]. The results from Transmission electron microscope (TEM), Field emission scanning electron microscope (FESEM) and Raman analyses indicate that bulk graphite has been extensively exfoliated to give single-layer and few-layer graphene nanoplates (Fig. 1S, Supporting information).

The nanocomposite microstructure was examined using XRD and TEM measurements. Fig. 2a shows XRD patterns of GA-2. The XRD features of GA-1 and GA-3 are similar. It is seen that almost all the diffraction peaks can be assigned to cubic phase of Ag_2O (JPCDS No. 41-1104) and hexagonal phase of graphite (JPCDS No. 75-1621). Remarkably, the peak intensities of graphene are obviously weakened as expected owning to the exfoliation of lamellar structure of bulk graphite in NMP. The most intense peak at around $2\theta = 26.5^\circ$ is speculated owning to the overlapped peaks of Ag_2O (1 1 0) and exfoliated graphene (0 0 2). These peaks of Ag_2O (26.65°) and graphene (26.23°) are so close to each other that we cannot make a clear distinction between them, and therefore only one well-resolved peak can be observed at around 26.5°. In addition, no peaks

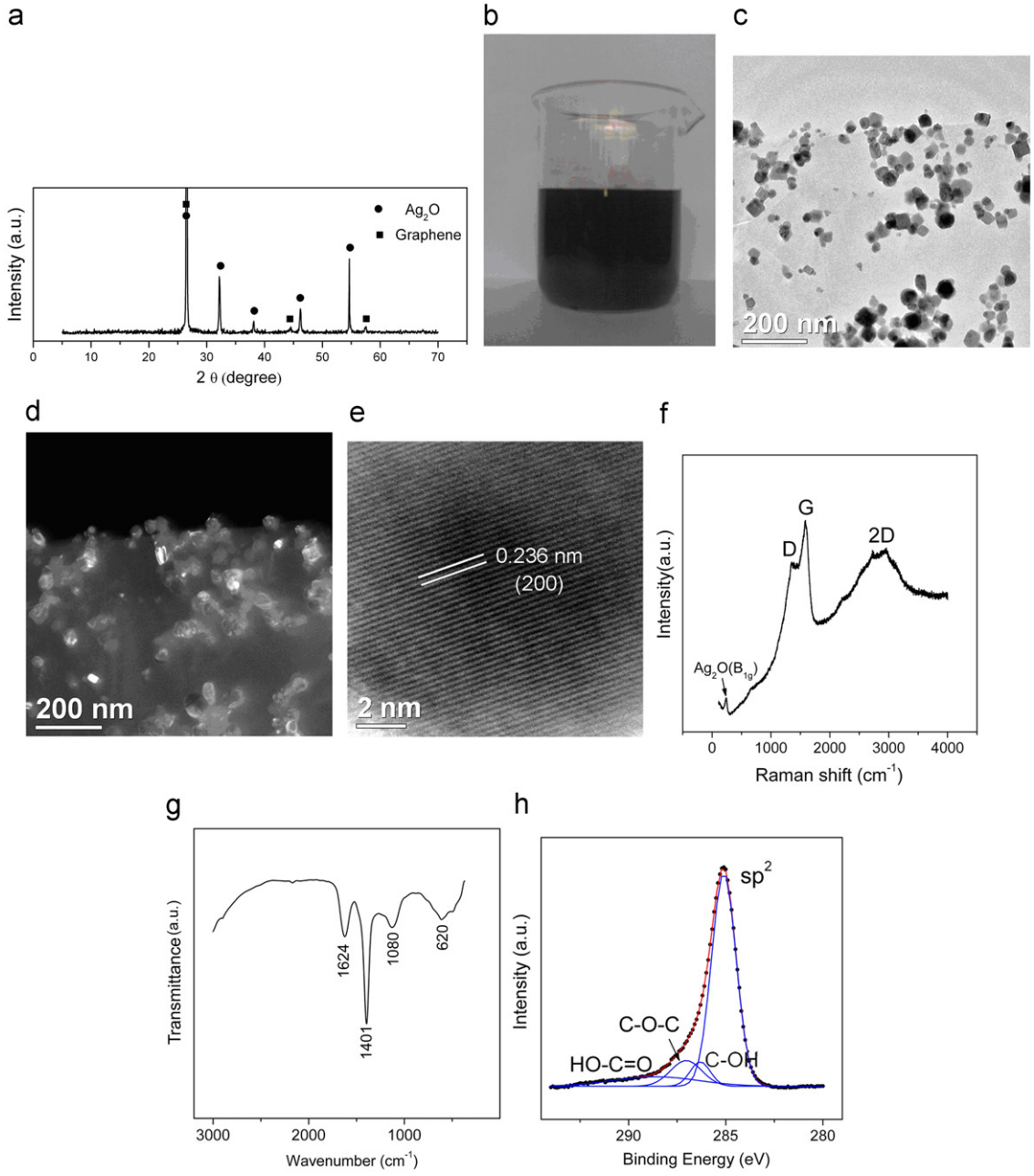

Fig. 2. (a) XRD patterns, (b) optical image, (c–e) TEM images, (f) Raman, (g) FT-IR and (g) XPS spectroscopy of GA-2.

attributable to other species indicate the high purity of the samples obtained.

In TEM images (Fig. 2c–e), the Ag_2O nanocrystals are highly dispersed on graphene sheets with the edges of supports clearly discerned from the background. The interplanar distance of approximately 0.236 nm is uniquely indexed as corresponding to the two nearest crystal planes (2 0 0) of Ag_2O, in good consistence with XRD results. Moreover, the stable colloidal nature of graphene–Ag_2O dispersion is highlighted by its optical images (Fig. 2b), enabling the possibility of using this *in situ* oxidation route to create new graphene-based materials and devices.

The soft oxidation degree nature of as-proposed *in situ* oxidation route is verified using Raman, FT-IR and XPS techniques. In Raman spectroscopy of GA-2 (Fig. 2f), there are three main bands around 1360, 1600 and 2700 cm^{-1}, corresponding to the breathing mode of κ-point phonons of $A1g$ symmetry (D band), the first-order scattering of the $E2g$ phonons (G band) and the second order of the D band (2D) of graphene, respectively [26]. The band at 220 cm^{-1} is ascribed to the B_{1g} characteristic scattering of Ag_2O, suggesting the existence of Ag_2O nanocrystals in the composite [27]. Additionally, the D/G peak intensity ratio of GA-2 is calculated to be 0.58, which is extensively lower than many graphene based composites obtained from GOs (in the range of 1.0–1.5) [10,16]. Commonly the intensity ratio of D band to G band can serve as a convenient measurement of the amount of defects in graphitic materials, and therefore the D/G intensity ratio is also relative to the incorporation level of functional groups into the carbon backbone [16,28], that is, a lower ratio corresponds to the graphene sheets having smaller functional groups. Accordingly, Raman spectroscopy indicates that relative small amount of functional groups was induced in the graphene frameworks.

It is worth mentioning that the Raman spectrum of GA-2 is different from that of bulk graphite. The D/G peak intensity ratio of GA-2 is relative higher than that of bulk graphite as expected due to edge effects from exfoliated graphene and the introduction of a small amount of oxygen-containing functional groups on graphene surfaces [23,29]. Generally the 2D peak in bulk graphite consists of two components; while only a single 2D peak observed in GA-2 indicate the exfoliation of bulk graphite to give mono and few layer graphene sheets. The presence of Ag_2O peak (220 cm^{-1}) signifies graphene and Ag_2O coexist in GA-2.

In FT-IR spectroscopy of GA-2 (Fig. 2g), a band around 1624 cm^{-1} is attributed to the stretching vibrations of carbon backbone of graphene; a band at 620 cm^{-1} represents the specific fingerprint of the Ag–O bond vibrations of Ag_2O, suggesting the coexistence of graphene and Ag_2O in the composite [30]. Moreover, the incorporation of some functional groups, like O–H deformation vibrations of C–OH (1401 cm^{-1}), C–O stretching vibrations of C–O–C (1080 cm^{-1}) are also observed. No noticeable absorption of carboxylate groups around 1700 cm^{-1} for GA-2 gives evidence of the low oxidation degree of graphene nanoplates.

The XPS spectroscopy of GA-2 (Fig. 1S) indicates that the product contains C, O and Ag as the main elements. In Fig. 2h, the C1s peak can be deconvoluted into four components at binding energies of 285.1 eV(C–C), 286.3 eV(C–OH), 287.0 eV (C–O–C), and 288.6 eV (HO–C═O). After integrating the area of each deconvoluted peak, the approximate percentage of introduced oxygen-containing groups

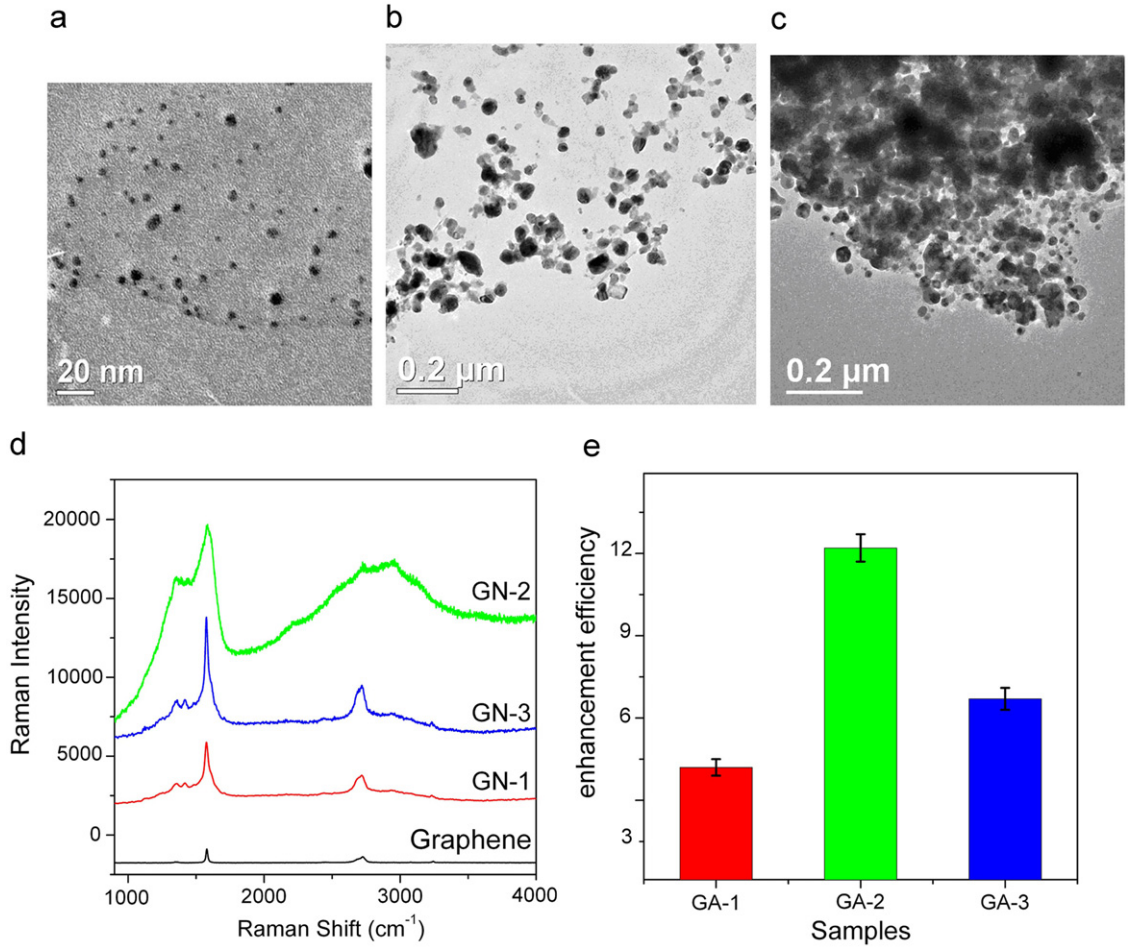

Fig. 3. TEM images of (a) GA-1, (b) GA-2 and (c) GA-3; (d) Raman spectra of graphene, GA-1, GA-2, and GA-3; (e) Enhancement efficiency of GA-1, GA-2, and GA-3.

(C–OH, C–O–C and HO–C= O) is 29.8%, much lower than that of GO (~50%) in previous published reports [13,31]. According to Raman, FT-IR, and XPS analyses, it is safe to conclude that our *in situ* oxidation route yields a relatively low amount of fragments and defects in graphene frameworks, indicating its soft oxidation nature [14,32].

It is well known that the microstructural features, such as size distribution, crystal morphology and dispersibility may play a vital key in the performances of nanoscale materials [33,34]. In this study, the microstructures of the as-obtained graphene–Ag_2O composite can be readily tailored by changing the synthetic parameters (please see Section 2), and as shown in Fig. 3a–c, the average sizes of Ag_2O for GA-1, GA-2 and GA-3 are 6, 40 and 45 nm, respectively; while there are more Ag_2O nanoparticles on graphene sheets for GA-3 than the others. Commonly, this phenomenon is related to the nuclei and crystal growth of Ag_2O crystals. It is reasonable that a higher concentration and long reaction time are beneficial to the nucleation and crystal growth process, giving rise to more Ag_2O crystals with larger particle sizes. The following results will verify that the optical and electrochemical performances of the composite can be tailored by this method.

Raman spectroscopy is a power technique to provide detailed information about molecular structures. However, recent Raman researches are circumscribed by its low sensitivity. Surface-enhanced Raman scattering (SERS) is able to overcome this disadvantage by giving a spectral intensity often enhanced by many orders of magnitude for molecules adsorbed on a properly fabricated metal (e.g., Ag, Au and Pt) surface. This facilitates the investigation of the structural and electronic properties of materials in detail [26]. It is generally accepted that two mechanisms are contributable to the SERS: the electromagnetic and the charge transfer mechanisms [35]. Another enhancement can also be acquired from molecular resonances, but they are only considered in specific system. The electromagnetic enhancement usually can contribute factors of about 10^4–10^6 to the Raman enhancement. While the charge transfer enhancement involves the chemisorption interaction and the metal–adsorbate charge transfer, and is usually said to contribute factors of about 10–100 of the observed enhancement.

It is known that silver oxide (Ag_2O) films can serve as excellent substrates for SERS for molecular sensing with high sensitivity and specificity due to the formation of photoinduced Ag clusters [36,37]. Given the unique 2D nanostructure, we can also regard these graphene sheets as monolayer molecules adsorbed on silver oxide-nanoparticle films. The Raman spectra of graphene, GA-1, GA-2, and GA-3 are compared in Fig. 3d. The intensities of the D, G, and 2D bands of graphene in composite systems obviously increase in comparison with those of the original graphene in the same test conditions. As a typical example, the enhancement efficiency of G band decreases in the following order (Fig. 3e), GA-2 > GA-3 > GA-1, implying that the nanocomposite microstructures exert a strong influence on the optical properties. Since the enhancement efficiency of GA-2 is evaluated in the range of 10–100, the charge–transfer mechanism is supposed to be responsible for this process [35]. It is thought that silver oxide nanoparticles adsorbed on graphene sheets could use the attached a small amount of functional

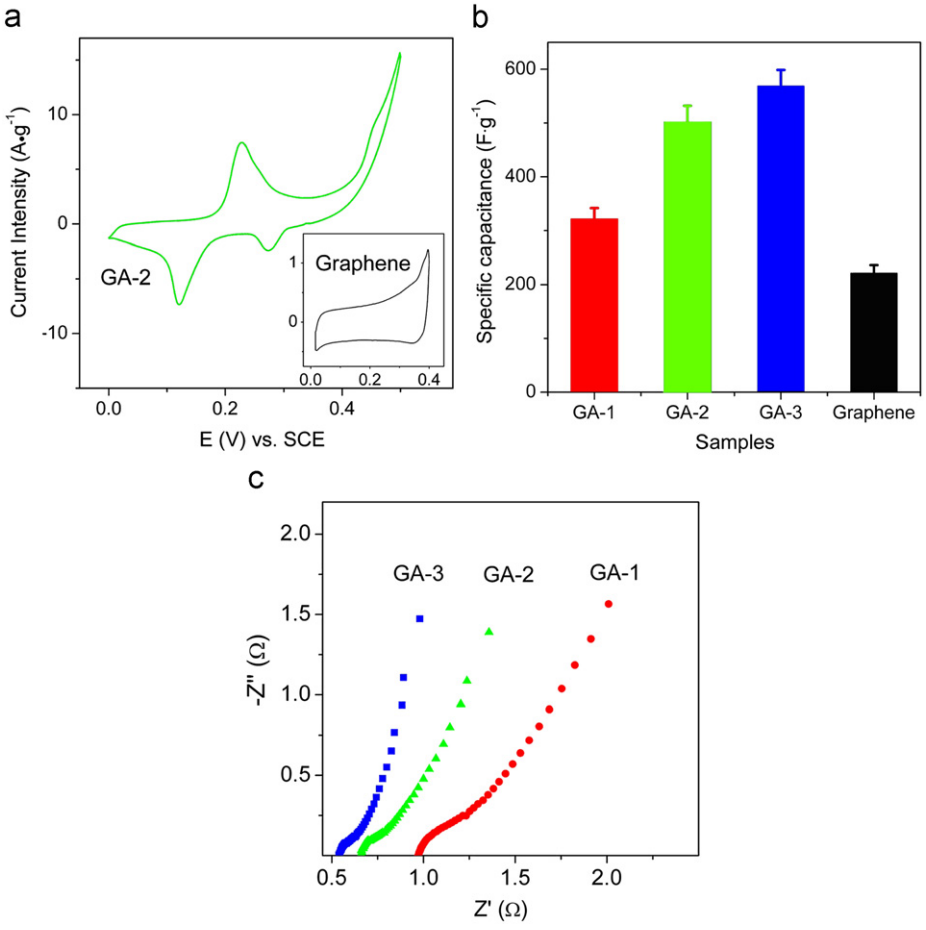

Fig. 4. (a) Cyclic voltammetry (CV) of GA-2 and graphene; (b) specific capacitance (C_s) of graphene, GA-1, GA-2, and GA-3; (c) EIS analyses of GA-1, GA-2, and GA-3.

groups as nucleation centers. According to the chemical mechanism of SERS, such interaction may form the charge–transfer complex, which can absorb light at the excitation frequency, consequently producing chemical SERS.

As mentioned above, the excellent conductivity of graphene sheets obtained from our approach can be maintained because of the small amount of defects and fragments. To explore the potential utilizations, the samples were fabricated into electrodes and the relevant electrochemical behavior was characterized by cyclic voltammetry (CV) and electrochemical impedance spectroscopy (EIS). Typical CV response of as-synthesized samples carried out at a scan rate of 5 mV s^{-1} is shown in Fig. 4a. The nearly rectangular CV curve of graphene nanoplates indicates the ideal capacitive nature of the fabricated electrode in strong alkaline electrolyte [22]. The obvious peaks in the CVs for GA-2 (the CVs of GA-1 and GA-3 are similar) is related to the redox reaction: $Ag_2O+H_2O+2e^- \rightarrow 2Ag+2OH^-$. Moreover, the specific capacitance (C_s) from the CVs was calculated based on the following equation,

$$C_s = \frac{1}{mv(V_f - V_i)} \int_{V_i}^{V_f} I(V)dV$$

where m is the mass of the active electrode material, v is the scan rate, V_f and V_i are the integration potential limits of the voltammetric curve, and $I(V)$ is the voltammetric current [38]. The C_s values of pristine graphene, GA-1, GA-2 and GA-3 are calculated to be 221.4, 321.8, 502.1 and 568.7 F g^{-1}, respectively (Fig. 4b). The CV results indicate that the electrochemical properties of the composite materials can be tailored in our synthetic conditions.

The EIS data of these samples was analyzed using Nyquist plots (Fig. 4c). The EIS plots of these samples contain a partially overlapped semicircle and a straight sloping line. Such a pattern of the plots can be fitted by an equivalent circuit in the inset of Fig. 2S (Supporting information), where the R_b is bulk resistance of the electrochemical system, R_{ct} is the Faradic charge–transfer resistance, and W is the Warburg impedance. In comparison with GA-1 and GA-2, GA-3 has a lower R_b (the intersection of the curve at real part Z' in the high frequencies range), R_{ct} (the semicircle at high frequencies) and the Warburg impedance (the slope of the curves at a low frequency). Such low values of R_b (0.51 Ω), R_{ct} (about 0.1 Ω calculated by the instrument), and W (as indicated by the precipitous slope at a low frequency) of GA-3 suggest it can be used as a promising electrode material for supercapacitors.

Based on the above results, GA-3 becomes the focus for further electrochemical characterization. GA-3 was subjected to galvanostatic charge–discharge measurements in a two-electrode device. Fig. 4Sa shows galvanostatic charge–discharge curves of GA-3 at different current densities (Supporting information). The C_s is calculated according to $C_s=I/[m(dV/dt)]$ from the discharge curves, where I is the constant discharge current, m is the mass of active materials, and dV/dt can be obtained from the slope of the discharge curve given by the instrument. The C_s of GA-3 at 200, 500, 800, and 1000 mA g^{-1} are 178.2, 146.5, 126.5 and 118.9 F g^{-1}, respectively. The decrease in capacitance with increase in discharge current suggests an increasing involvement of polarization, a phenomenon that results in a low utilization of the active materials at higher charge/discharge currents [39]. Moreover, these values are lower than that obtained from CVs

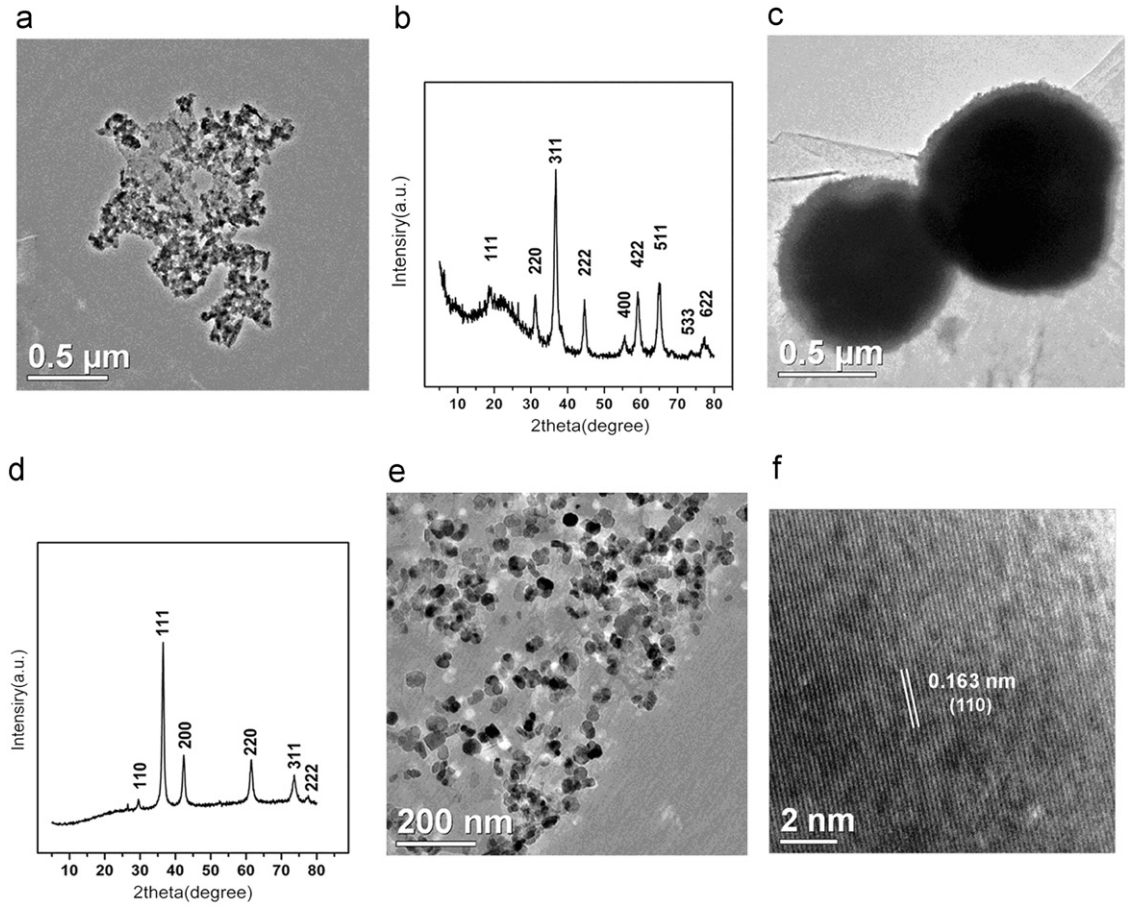

Fig. 5. TEM images of graphene–Co_3O_4 (a), Cu_2O (c), and ZnO (e, f) composites; XRD patterns of graphene–Co_3O_4 (b), Cu_2O (d) composites.

in a three-electrode cell. This phenomenon is reasonable and attributable to the different applied voltage and charge transfer of an electrode in the two- or three electrode cell configuration [40]. Generally, for a three-electrode cell, the voltage potential applied to the working electrode is equal to the values shown on the X-axis of the CV chart, while in a symmetrical two-electrode cell, the potential differences applied to each electrode are equal to each other and are only one-half of the values shown on the X-axis of the CV chart. Therefore, the C_s calculated from a two-electrode cell is usually less than half of that obtained from a three-electrode cell [40].

Furthermore, the electrochemical stability of GA-3 in a two-electrode cell is studied. Unfortunately, the electrode showed poor cycle ability (with only 54.6% at 1000 mA g^{-1} for 500 cycles). Therefore, a number of problems remain to be solved before practical use.

As indicated earlier in this article, graphene–Ag_2O hybrids can be obtained under ambient conditions due to the hydrolysis of $AgNO_3$ aqueous solution in the presence of NMP at room temperature. Nevertheless, the hydrolysis of $Co(NO_3)_2$, $Cu(NO_3)_2$ and $Zn(NO_3)_2$ is quite slow under the same conditions, therefore the accelerated hydrolysis was carried out at higher temperatures to decorate graphene sheets with Co_3O_4, Cu_2O and ZnO nanoparticles, respectively. Specifically, the solvothermal treatment was applied at 180 °C for 2 h for $Co(NO_3)_2$, while $Cu(NO_3)_2$, and $Zn(NO_3)_2$ were subjected to refluxing at 120 °C for 2 h. The XRD patterns (Fig. 5b and d) indicated that the crystal forms of Co_3O_4 (JPCDS No. 78-1970), Cu_2O (JPCDS No. 78-2076), and ZnO (JPCDS No. 05-0664, not shown here) were obtained. It can be clearly seen from Fig. 5a,c and e that all the metal oxide nanoparticles have been attached onto graphene sheets. Additionally, the lattice fringes with interplanar distance of approximately 0.163 nm correspond to the (1 1 0) plane of the hexagonal (Wurtzite) ZnO (Fig. 5f), consistent with XRD patterns. The above results imply that our approach is worth promoting and can be applied to synthesize a series of graphene nanoplate–metal oxide nanocomposites.

4. Conclusions

In this work, we demonstrate a soft oxidation route to fabricate a series of graphene nanoplate–metal oxide nanocomposites. The hydrolysis of metal nitrate precursors is a key step throughout the whole process. By controlling the reaction parameters, optical and electrochemical performances of the composite are successfully tailored. Relatively lower amounts of fragments and defects introduced in the preparation process may open up brand new applications for hybrids on the basis of this amazing material. Moreover, taking into account the easy synthesis and straightforward nature of our procedure, we hope this work can push the potential utilizations of graphene to a broader horizon.

Acknowledgments

This investigation was supported by the Natural Science Foundation of China and China Academy of Engineering Physics (No. 10776014 and 50902070), the Natural Science Foundation of Jiangsu Province (No. BK2009391), the Research Fund for the Doctoral Program of Higher Education of China (No. 20093219120011), and NUST Research Funding, NO. ZDJH07.

Appendix A. Supporting information

Supplementary data associated with this article can be found in the online version at doi:10.1016/j.jssc.2011.03.054.

References

[1] K.S. Novoselov, A.K. Geim, S.V. Morozov, D. Jiang, Y. Zhang, S.V. Dubonos, I.V. Grigorieva, A.A. Firsov, Science 306 (2004) 666–669.
[2] A.K. Geim, K.S. Novoselov, Nat. Mater. 6 (2007) 183–191.
[3] B.B. Athanasios, G. Vasilios, Z. Radek, A.S. Theodore, K.S. Athanasios, Small 5 (2009) 1841–1845.
[4] S. Bae, H. Kim, Y. Lee, X. Xu, J.-S. Park, Y. Zheng, J. Balakrishnan, T. Lei, H. Ri Kim, Y.I. Song, Y.-J. Kim, K.S. Kim, B. Ozyilmaz, J.-H. Ahn, B.H. Hong, S. Iijima, Nat. Nanotechnol. 5 (2010) 574–578.
[5] X. Li, W. Cai, J. An, S. Kim, J. Nah, D. Yang, R. Piner, A. Velamakanni, I. Jung, E. Tutuc, S.K. Banerjee, L. Colombo, R.S. Ruoff, Science 324 (2009) 1312–1314.
[6] K.S. Kim, Y. Zhao, H. Jang, S.Y. Lee, J.M. Kim, K.S. Kim, J.-H. Ahn, P. Kim, J.-Y. Choi, B.H. Hong, Nature 457 (2009) 706–710.
[7] Z. Weixia, C. Jiecheng, T. Cheng-an, W. Yiguang, L. Zhanping, M. Li, W. Yuquan, L. Guangtao, Angew. Chem. Int. Ed. 48 (2009) 5864–5868.
[8] D. Li, M.B. Muller, S. Gilje, R.B. Kaner, G.G. Wallace, Nature 3 (2008) 101–105.
[9] S. Stankovich, D.A. Dikin, K.M. Kohlhaas, E.J. Zimney, E.A. Stach, R.D. Piner, S.T. Nguyen, R.S. Ruoff, Nature 442 (2006) 282–286.
[10] S. Chen, J. Zhu, X. Wu, Q. Han, X. Wang, ACS Nano 4 (2010) 2822–2830.
[11] C. Aoneng, L. Zhen, C. Saisai, W. Minghong, Y. Zhangmei, C. Zhengwei, C. Yanli, W. Shufeng, G. Qihuang, L. Yuanfang, Adv. Mater. 22 (2010) 103–106.
[12] C. Xu, X. Wang, J. Zhu, J. Phys. Chem. C 112 (2008) 19841–19845.
[13] D.W. Boukhvalov, M.I. Katsnelson, J. Am. Chem. Soc. 130 (2008) 10697–10701.
[14] H.K. Jeong, Y.P. Lee, R.J.W.E. Lahaye, M.H. Park, K.H. An, I.J. Kim, C.W. Yang, C.Y. Park, R.S. Ruoff, Y.H. Lee, J. Am. Chem. Soc. 130 (2008) 1362–1366.
[15] D.W. Lee, L. De Los Santos V, J.W. Seo, L.L. Felix, A. Bustamante D, J.M. Cole, C.H.W. Barnes, J. Phys. Chem. B 114 (2010) 5723–5728.
[16] S. Park, R.S. Ruoff, Nat. Nanotechnol. 4 (2009) 217–224.
[17] C. Xu, X. Wang, J. Zhu, X. Yang, L. Lu, J. Mater. Chem. 18 (2008) 5625–5629.
[18] L.-I. Hung, C.-K. Tsung, W. Huang, P. Yang, Adv. Mater. 22 (2010) 1910–1914.
[19] W. Zou, J. Zhu, Y. Sun, X. Wang, Mater. Chem. Phys. 125 (2011) 617–620.
[20] X. Wang, H.-F. Wu, Q. Kuang, R.-B. Huang, Z.-X. Xie, L.-S. Zheng, Langmuir 26 (2010) 2774–2778.
[21] V. Chandra, J. Park, Y. Chun, J.W. Lee, I.-C. Hwang, K.S. Kim, ACS Nano 4 (2010) 3979–3986.
[22] M.D. Stoller, S. Park, Y. Zhu, J. An, R.S. Ruoff, Nano Lett. 8 (2008) 3498–3502.
[23] Y. Hernandez, V. Nicolosi, M. Lotya, F.M. Blighe, Z. Sun, S. De, I.T. McGovern, B. Holland, M. Byrne, Y.K. Gun'Ko, J.J. Boland, P. Niraj, G. Duesberg, S. Krishnamurthy, R. Goodhue, J. Hutchison, V. Scardaci, A.C. Ferrari, J.N. Coleman, Nat. Nanotechnol 3 (2008) 563–568.
[24] L. Hu, J.W. Choi, Y. Yang, S. Jeong, F. La Mantia, L.F. Cui, Y. Cui, Proc. Natl. Acad. Sci. U. S. A. 106 (2009) 21490–21494.
[25] W. Zhou, H. Liu, J. Wang, D. Liu, G. Du, J. Cui, ACS Appl. Mater. Interf. 2 (2010) 2385–2392.
[26] A.C. Ferrari, Solid State Commun. 143 (2007) 47–57.
[27] B.J. Murray, Q. Li, J.T. Newberg, J.C. Hemminger, R.M. Penner, Chem. Mater. 17 (2005) 6611–6618.
[28] S. Stankovich, D.A. Dikin, R.D. Piner, K.A. Kohlhaas, A. Kleinhammes, Y. Jia, Y. Wu, S.T. Nguyen, R.S. Ruoff, Carbon 45 (2007) 1558–1565.
[29] A. Ferrari, Solid State Commun. 143 (2007) 47–57.
[30] R.C. Lucacel, C. Marcus, V. Timar, I. Ardelean, Solid State Sci. 9 (2007) 850–854.
[31] P. Renu, G. Shweta, S.Avanish Kumar, Small 5 (2009) 2253–2259.
[32] N.I. Kovtyukhova, P.J. Ollivier, B.R. Martin, T.E. Mallouk, S.A. Chizhik, E.V. Buzaneva, A.D. Gorchinskiy, Chem. Mater. 11 (1999) 771–778.
[33] X. Fu, F. Bei, X. Wang, X. Yang, L. Lu, J. Raman Spectrosc. 41 (2010) 370–373.
[34] S. Devaraj, N. Munichandraiah, J. Phys. Chem. C 112 (2008) 4406–4417.
[35] X. Fu, F. Bei, X. Wang, S. O'Brien, J.R. Lombardi, Nanoscale 2 (2010) 1461–1466.
[36] M. Fujimaki, Y. Iwanabe, K. Awazu, J. Tominaga, Microelectron. Eng. 83 (2006) 1626–1629.
[37] X. Wang, H. Wen, T. He, J. Zuo, C. Xu, F.-C. Liu, Spectrochim. Acta A 53 (1997) 2495–2504.
[38] Z.-S. Wu, D.-W. Wang, W. Ren, J. Zhao, G. Zhou, F. Li, H.-M. Cheng, Adv. Funct. Mater. 20 (2010) 3595–3602.
[39] G. Hu, C. Li, H. Gong, J. Power Sources 195 (2010) 6977–6981.
[40] M.D. Stoller, R.S. Ruoff, Energy Environ. Sci. 3 (2010) 1294–1301.